www.springer.com/41230
https://doi.org/10.1007/s41230-025-4203-1
Research & Development
Vol. 23 No. 2 March 2026
CHINA FOUNDRY

# Stress-rupture behavior of a Ni-based Re-containing single crystal superalloy in [001] and [111] orientations at 1100 °C

**Guang-lei Wang[1], Dong-qing Qi[2], *Jin-lai Liu[1], and **Ji-de Liu[1]**
*1. Institute of Metal Research, Chinese Academy of Sciences, Shenyang 110016, China*
*2. School of Chemistry and Chemical Engineering, Shandong University, Jinan 250100, China*

**Abstract:** Turbine blades, due to their intricate geometry, are exposed to multiaxial stresses during operation. Consequently, it is imperative to examine the anisotropy of their stress-rupture behavior across various testing scenarios, particularly under high-temperature conditions. Stress-rupture behavior of a Ni-based single crystal superalloy was investigated under a load varying from 100 MPa to 137 MPa at 1,100 °C for both [001]- and [111]-orientated specimens. Results demonstrate that the rupture behavior of [111]-orientated specimens exhibits obviously higher sensitive to applied stress compared to [001]-orientated specimens. This difference is primarily attributed to the orientation dependent γ′ coarsening behavior and distinct dislocation interactions at γ/γ′ interfaces. In [001]-oriented specimens, plate-like γ/γ′ rafts rapidly form alongside well-developed interfacial dislocation networks, where the γ/γ′ misfit stress dominates the microstructural evolution. In contrast, the [111]-orientated specimens exhibit retained, coarsened γ′ precipitates embedded within the γ matrix, accompanied by poorly developed interfacial dislocation networks.

**Keywords:** Ni-based single crystal superalloy; stress-rupture behavior; deformation mechanism; stress dependence; orientation dependence

**CLC numbers:** TG146.1$^{+}$5 **Document code:** A **Article ID:** 1672-6421(2026)02-179-07

## 1 Introduction

Ni-based single crystal superalloys with the compound γ/γ' structure are widely employed in advanced aero-engine turbine blades and vanes due to their excellent creep (stress-rupture) resistance at elevated temperatures[1]. The intricate geometries of these components impose multiaxial stress states during operation. Therefore, it is crucial to investigate how their stress-rupture behavior varies with anisotropy in different testing environments, especially at elevated temperatures[2].

In general, at intermediate temperatures, Ni-based single crystal superalloys exhibit a highly orientation-dependent stress-rupture behavior under high stresses, but much weaker at low stresses[3-5]. The initial γ′ size is one of the key factors for the creep anisotropy of several alloys under high stresses at relatively low temperatures, though its influence is reduced when the temperature increases[6]. Notably, stress-rupture anisotropy persists even at high temperatures, especially in [001] and [111] orientations[3-11]. It shows contradictory results in different alloys along these two loading directions under various testing conditions. For instance, the [111]-orientated crystals of CMSX-4 exhibit poor creep resistances below 5% strain under 980 °C/350 MPa, compared to [001] orientated ones[7]. It is found in a Ni-based Re-free alloy that the creep-fracture lifetime in [111]-orientated specimens is shorter than [001]-orientated ones under 1,040 °C/160 MPa[8]. However, an opposite observation is found in a Ni-based Re-doping alloy under conditions of 1,100 °C/100 MPa[9]. The stress-rupture behaviors in both [001] and [111] orientations are closely dependent on the testing conditions, especially the applied stress. However, the extent to which stress levels influence high-temperature stress-rupture behavior in [001]- and [111]-oriented single-crystal alloys, as well as the

***Jin-lai Liu**
Male, born in 1973, Assistant Professor. His research interests are mainly focused on design of single crystal superalloys and characterization of microstructures of superalloys.
E-mail: jlliu@imr.ac.cn
****Ji-de Liu**
E-mail: jdliu@imr.ac.cn

Received: 2024-09-22; Revised: 2024-10-28; Accepted: 2024-11-04

underlying mechanisms driving this anisotropy, remains unresolved and warrant further investigation.

Based on the above considerations, in the present study, the microstructural evolution after heat treatment associated with stress-rupture behavior was investigated in a Ni-based superalloy with [001] and [111] single crystals at 1,100 °C, subjected to different applied loads of 100 MPa and 137 MPa. The objective was to elucidate the differential effects of stress level on rupture mechanisms and the underlying deformation processes in both [001]- and [111]-loading directions.

## 2 Experimental procedure

The Ni-based single crystal superalloy used in this study had a composition of Ni, 7.5 Co, 6.9 Cr, 6.2 Al, 6.5 Ta, 5.0 W, 1.5 Mo, 3.0 Re, 0.05 C (wt.%). On the industry scale, Ni-based single crystal superalloys were actually prepared using crystal-selection and seed-crystal methods. In particular, the [001]-oriented single crystal rods were produced with the spiral crystal selection technique, while the single crystal rods with [111] orientation were grown on pre-fabricated seeds which were cut from the [001]-orientated single crystals without solidification defects. After conducting the macroscopic corrosion inspection, the radial orientation of individual single crystal rod was determined using electron backscatter diffraction (EBSD) technology. Single-crystal bars exhibiting an orientation deviation of ≤10° from the [001] or [111] orientation were selected for subsequent heat-treatment experiments. The heating treatment included a homogenization treatment [1,310 °C/2 h, air cooling (AC)] and a two-step aging treatment (1,130 °C/4 h, AC+ 900 °C/16 h, AC). The heat treating schedule and resultant microstructure have been given in Ref. [12]. It should be noted that the industrial-scale Ni-based single crystal superalloys contain numerous as-solidified dendrites separated by low-angle grain boundaries formed during the directional solidification process. Diffraction contrast results indicate the misorientations between dendrites can reach up to 3°, localized in the interdendritic regions in the as-solidified state[13].

Cylindrical samples machined from the heat-treated rods had a gauge length of 25 mm and a gauge diameter of 5 mm. These samples were tested in tension until fracture under 100 MPa and 137 MPa, respectively at 1,100 °C in the atmosphere. The final result was an average of two samples ruptured under each testing condition. Fractured specimens were ultrasonically cleaned in ethanol for 15 min and then the fracture morphologies were observed using a tungsten filament scanning electron microscope (SEM, S-3400N) with an operating voltage of 20 kV. Metallographic specimens on the longitudinal section were cut from the ruptured samples by spark erosion. Then, they were prepared by mechanical grinding and polishing, followed by final chemically etched in a reagent composed of 4 g $Cu_2SO_4$, 20 mL $H_2O$, and 20 mL HCl at room temperature. Observations of γ/γ′ microstructure after fracture were conducted using a field emission SEM (Inspect F50) with an operating voltage of 30 kV. Thin discs were cut approximately 3 mm from the fracture surface using spark erosion. These foils were mechanically ground and then electrochemically thinned at about −15 °C in the solution of 10vol.% perchloric acid. Configurations of dislocations were implemented using transmission electron microscopy (TEM, JEOL 2100) operating at 200 kV.

## 3 Results

### 3.1 Comparison on macro-properties of single crystal superalloys in two orientations

Experimental results including the stress-rupture lifetime and elongation of [001]- and [111]-orientated specimens under stresses of 100 MPa and 137 MPa at 1,100 °C are shown in Fig. 1. It is clear that the rupture lifetime of this alloy is sensitive to the stress in both orientations and the rupture lifetime decreases as the stress increases. The decline of lifetime is 75.1% in [001]-orientated specimens, while this decline is as high as 92.0% in [111]-orientated specimens. Relatively speaking, the elongation has a negligible variation under different stresses in [001]-orientation. However, the [111]-oriented specimens demonstrate exceptional ductility with increasing stress, exhibiting an elongation enhancement of up to 516%. In addition, except the elongation in the [001] orientation, it is interesting that the rupture lifetime and elongation show a completely reversal trend with the increase of stress.

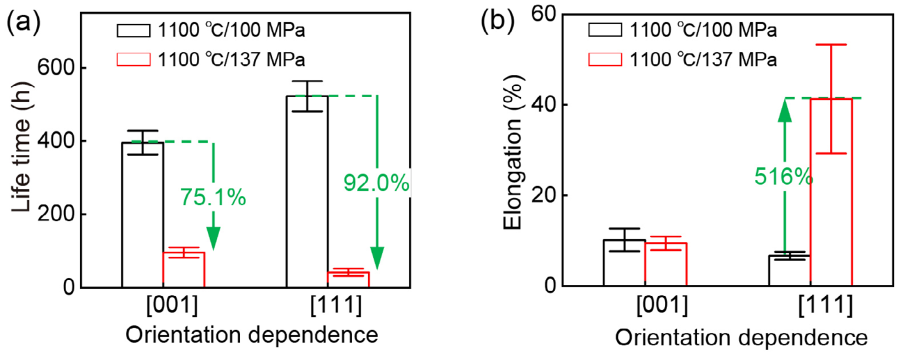

Fig. 1: Stress-rupture properties in [001] and [111] orientations under different stress levels at 1,100 °C: (a) lifetime; (b) elongation

## 3.2 Microstructural evolution

Microstructures observed by SEM in [001]- and [111]-orientated specimens after fracture under 1,100 °C/100 MPa are represented in Fig. 2. Figures 2(a) and (c) show the microstructures located at the position 4 mm from the fracture. Figures 2(b) and (d) display the microstructure near the fracture. Degradation of the γ/γ′ microstructure is observed in both oriented specimens at 1,100 °C; however, the resulting γ′ morphologies differ significantly between the two orientations. The morphology of the γ′ phase exhibits significant positional variation within the [001]-oriented specimen. For instance, the plate-like γ′ rafts remain intact in Fig. 2(a), whereas in Fig. 2(b), the rafted γ′ structure is fragmented, showing an inclination of 45° relative to the load direction. In contrast, in the [111]-oriented specimen, several closely spaced γ′ precipitates coalesce along the <100> direction [Figs. 2(c) and (d)]. It can also noted that the size of γ′ precipitate in Fig. 3 reaches 1–2 μm, while that of the primary γ′ precipitate is only about 0.45 μm[12]. The coarsened γ′ particles are still surrounded by γ matrix. The coarsening behavior of γ′ precipitates is obvious to some extent in the vicinity of the fracture where a high local strain is accumulated. Compared with [001]-orientated specimen, the γ channel is consistently narrower at the same position on the fracture surface in the [111]-orientated specimen.

Morphologies of γ/γ′ microstructure in [001]- and [111]-orientated specimens after fracture under 1,100 °C/137 MPa are generally similar to those in Fig. 2, which are not mentioned here. The evident difference is that the thickness period of the γ/γ′ rafts is decreased in both orientations with the increase of stress.

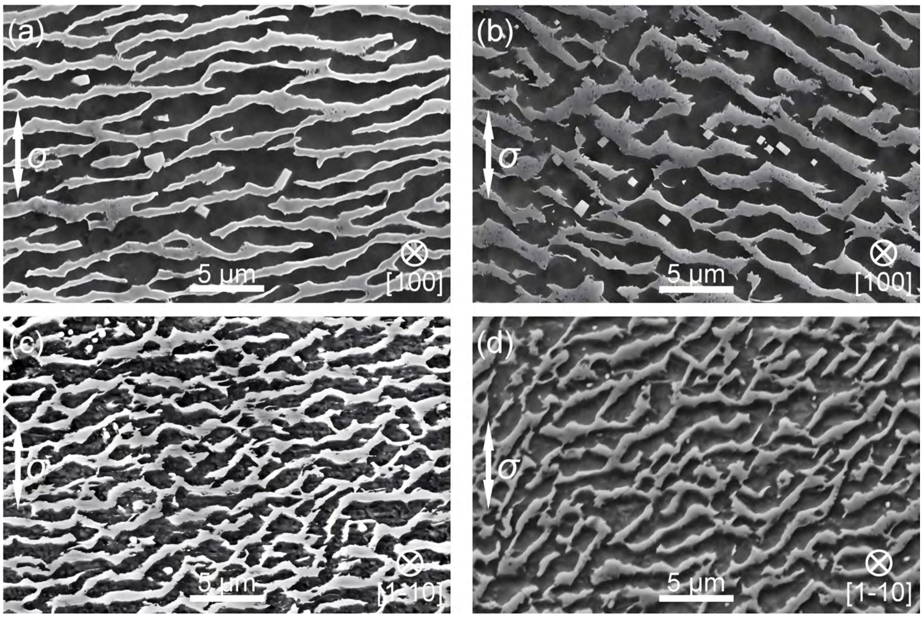

**Fig. 2: SEM micrographs of γ/γ′ microstructure located at different positions on longitudinal section from the fracture surface under 1,100 °C/100 MPa: (a) and (b) [001] orientation; (c) and (d) [111] orientation; (a) and (c) 4 mm away from the fracture surface; (b) and (d) near the fracture surface**

## 3.3 Comparison on typical dislocation configurations

Dislocation configurations in [001]- and [111]-orientated specimens after fracture under 1,100 °C/100 MPa were detected by TEM under various two-beam conditions (Fig. 3). The density of dislocations accumulated at the γ/γ′ interfaces and the magnitude/direction of the Burgers vectors of dislocations within the γ′ phase exhibit clear variations with the applied load direction. The dislocation networks are well refined with hexagonal and square shapes, resulting from dislocation interactions on (001) γ/γ′ interfaces in the [001]-orientated specimens. The straight segments in the insert part in Fig. 3(a) include *a*/2(110) and *a*(010) dislocations, both exhibiting edge character. Dislocations exhibiting oscillating contrasts under *g*=020 possess short projection segments in the middle part in Fig. 3(a) and are identified as *a*/2<101> dislocations with screw character in γ′ phase. As shown in Fig. 3(b), the superdislocation with a double residual contrast under *g*=002 is indeed identified as *a*<010> with edge character, which agrees with the previous findings[14, 15]. In addition, the *a*/2<101> dislocation pairs coupled by antiphase boundary (APB) are always found to be lying on cubic planes, not on octahedral planes. While, in [111]-orientated specimens, two groups of parallel long dislocations of 60° character are deposited at every type of γ/γ′ interfaces [Fig. 3(c)]. These long interfacial dislocations exhibit relatively wide spacing. The zigzag appearance of long dislocations is resulted from cross slip of dislocation loops of screw character within γ channels. A superdislocation with a Burgers vector of *a*<101> exhibits a Kear-Willsdort (K-W) configuration in γ′ phase, as shown at the right part in Fig. 3(d), the segments A and C are both on (11−1) plane and the segment B is on (100) plane. It should be noted that the *a*<010> superdislocations are hardly found in γ′ phase due to the poor-developed interfacial dislocation networks.

Representative microstructures of [001]- and [111]-orientated specimens after fracture under 1,100 °C/137 MPa are also detected by TEM, as shown in Fig. 4. The densities of dislocations in $\gamma/\gamma'$ microstructure, especially within $\gamma'$ phase, are both raised in both tensile loadings, especially in tensile deformation of [111]-orientated specimens. Dislocations with a Burgers vector of $a$/2<101> are frequently observed in $\gamma'$ plates in [001]-orientated specimens [Figs. 4(a) and (b)]. The $\gamma/\gamma'$ interfaces are covered with parallel long dislocations, as shown in Fig. 4(c). The bent shapes of the superdislocation segments suggest that they glide in the octahedral planes in $\gamma'$ phase, as shown in Figs. 4(c) and (d).

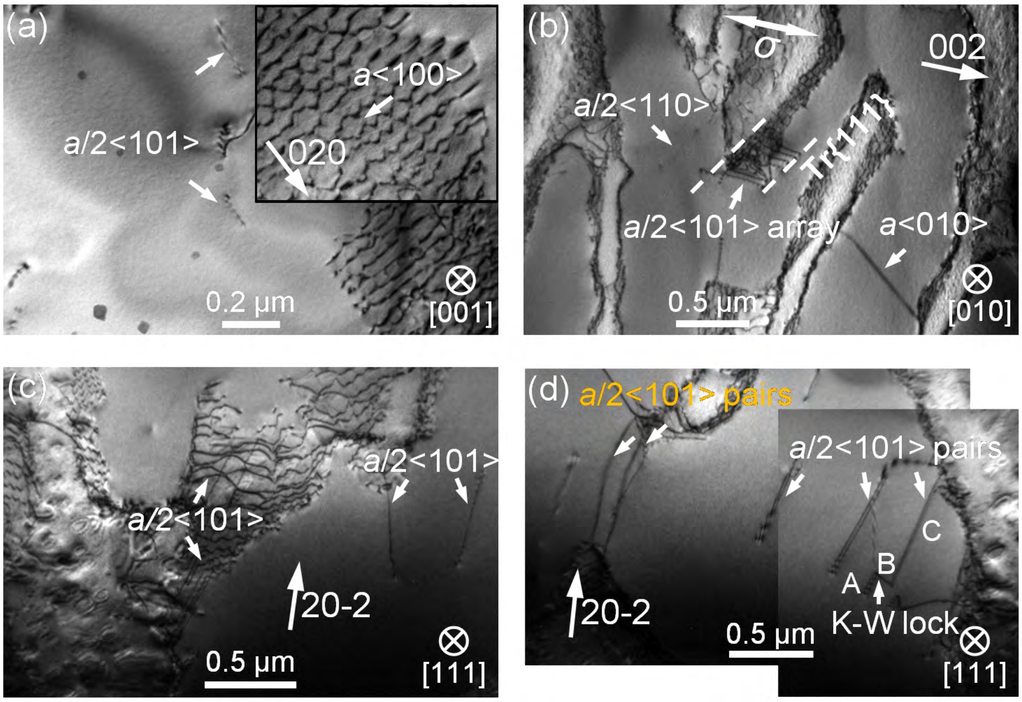

**Fig. 3: Bright field TEM images of dislocations under various two-beam conditions after fracture under 1,100 °C/100 MPa: (a) and (b) [001] orientation; (c) and (d) [111] orientation; (a) (001) plane; (b) (010) plane; (c) and (d) (111) planes**

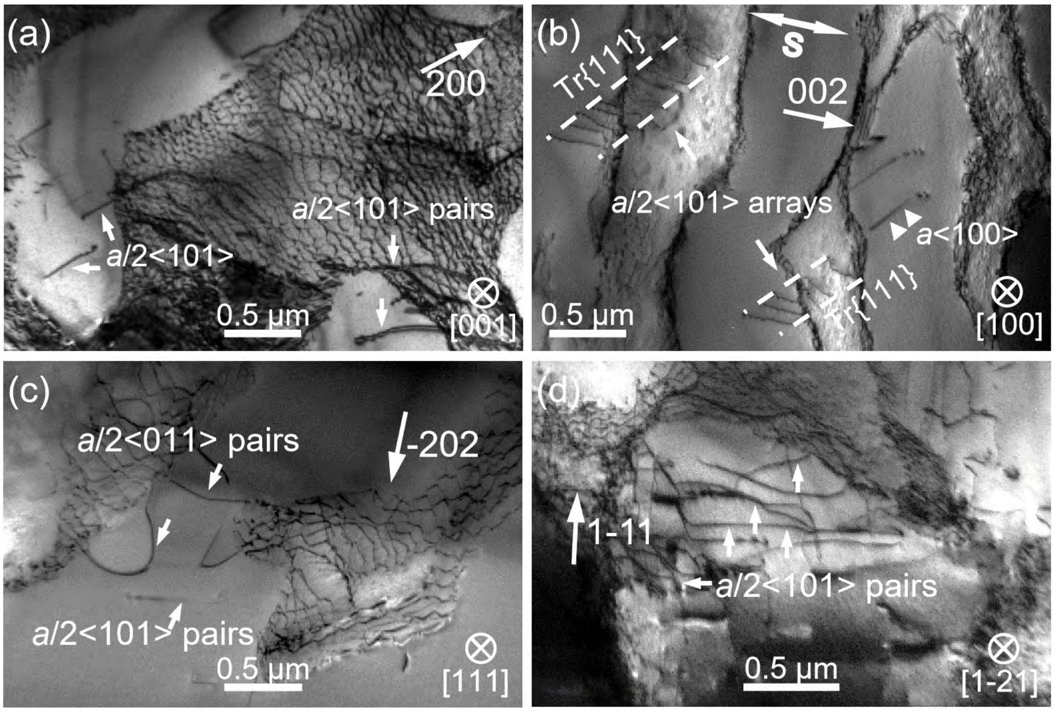

**Fig. 4: Bright field TEM images of dislocations under various two-beam conditions after fracture under 1,100 °C/137 MPa: (a) and (b) [001] orientation; (c) and (d) [111] orientation; (a) (001) plane; (b) (010) plane; (c) (111) plane; and (d) (1–21) planes**

### 3.4 Analysis of fracture surface

Fracture surfaces of [001]- and [111]-oriented specimens, observed by SEM after fracture under 1,100 °C/100 MPa conditions, are shown in Fig. 5. The fracture surfaces also differ in orientation. The fracture surface is roughly normal to the applied load direction in the [001] orientated specimens [Fig. 5(a)] and consisted of abundant creep dimples surrounded with small tearing edges [Fig. 5(b)]. Comparatively, the general fracture surface exhibits dendritic morphologies in the [111]-orientated specimens, as seen in Figs. 5(c) and (d). It corresponds well with the presence of low-angle grain boundaries in the industrial scale single crystals. A few creep dimples are observed on the fracture surface.

When the applied stress increases to 137 MPa, plentiful creep dimples are found on the fracture surfaces of the ruptured specimens in two orientations. The whole fracture surface is still perpendicular to the direction of applied load, as shown in Fig. 6(a), and the near-tetragonal creep dimples are frequently observed in the [001] orientated specimen, as shown in Fig. 6(b). While, the fracture surface in the [111]-orientated specimen shows a triangular-prism shape [Fig. 6(c)], corresponding to the macroscopic slipping planes. As present in Fig. 6(d), small near-trigonometric creep dimples with a low density are located at various heights on the fracture surface.

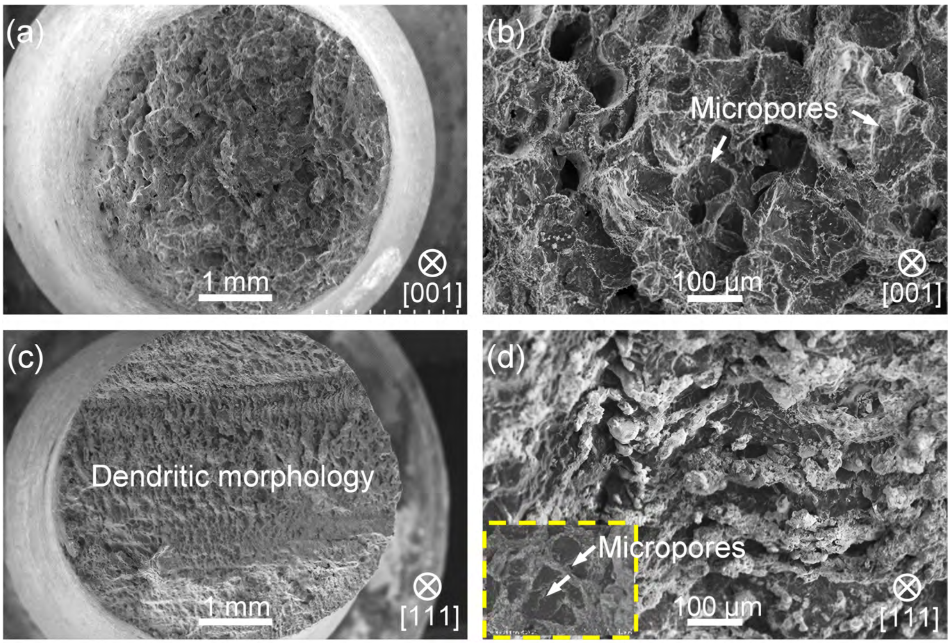

**Fig. 5: SEM micrographs of fracture morphologies of specimens with different orientations under 1,100 °C/100 MPa: (a) and (b) [001] orientation; (c) and (d) [111] orientation; (a) and (c) low magnitude; (b) and (d) high magnitude**

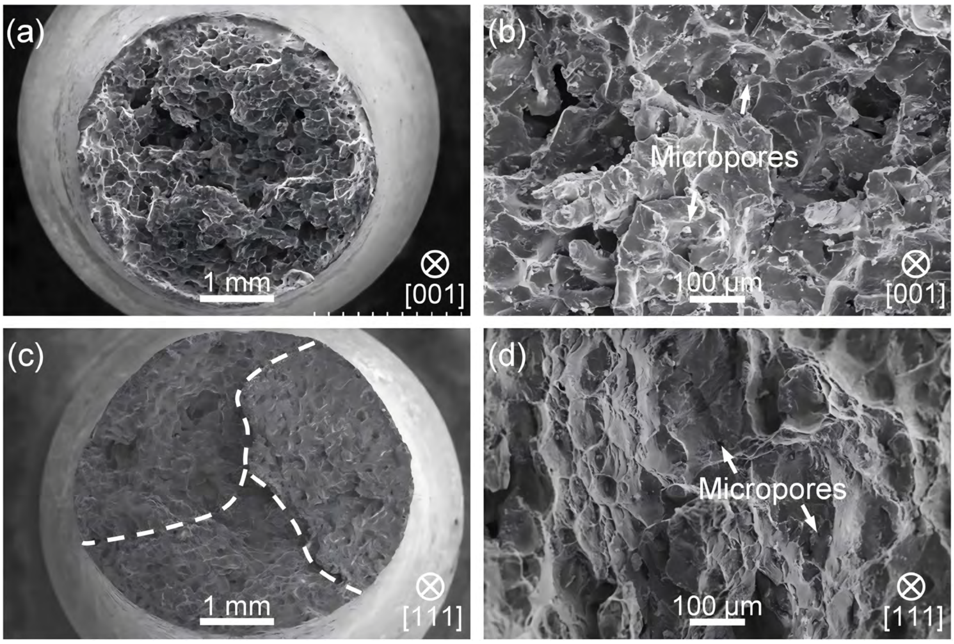

**Fig. 6: SEM micrographs of fracture morphologies of specimens with different orientations under 1,100 °C/137 MPa: (a) and (b) [001] orientation; (c) and (d) [111] orientation; (a) and (c) low magnitude; (b) and (d) high magnitude**

# 4 Discussion

## 4.1 Effect of γ/γ′ misfit stress on microstructural evolution

Deformation mechanisms associated with stress-rupture behavior of Ni-based single crystal superalloy at high temperatures are mainly controlled by the coarsening behavior of γ/γ′ microstructure and the development of dislocation networks around γ′ particles, in which the crystallographic structure, as well as the γ/γ′ lattice misfit, plays key roles[9-11]. Therefore, it is necessary to discuss the influence of γ/γ′ misfit stress on the basic deformation processes during [001] and [111] tensile deformation.

The coarsening behavior of γ′ precipitates is closely linked with the distribution of plasticity within γ channels, which varies with applied loading direction. The effect of γ/γ′ misfit stress on initial microscopic stress in γ channels upon application of load[16, 17]. Under the action of γ/γ′ misfit stress, the initial stress level is much bigger in the (001) γ channel than in the (100) and (010) γ channels in [001] orientation; while due to the high symmetry, all γ channels are under an identical initial stress level in [111] orientation. Correspondingly, dislocation multiplication is mainly activated in the (001) γ channel, which results in the occurrence of directional coarsening of γ′ precipitates at the early stage of [001] tensile loading (e.g., Ref. [18]). The γ′ rafting is accompanied by the closing of (100) and (010) γ channels and finally a lamella γ/γ′ raft structure is quickly attained at 1,100 °C. The kinetics of this process are minimally influenced by the applied stress level (e.g., Ref. [19]). However, due to the high symmetry, the three types of γ channels are all under an identical internal stress level and it suggests an Ostwald ripening of γ′ phase takes place due to the same plasticity in all γ channels during deformation along [111] orientation. It should be noted that the three types of γ channels are remained and the coarsened γ′ precipitates are still embedded in γ matrix.

The formation of dislocation networks at γ/γ′ interfaces is crucial for the elastic instability of γ′ precipitates and the γ′-cutting events by dislocations during further deformation, which also vary with the applied stress axis[20]. This suggests that deformation loading in the [001] direction can be associated with up to eight activated microscopic octahedral slip systems with a high Schmid factor (~0.41). It facilitates the dislocation interactions, leading to the formation of complete γ/γ′ interfacial dislocation networks that mostly exhibit an edge character, as seen in Figs. 3(a) and 4(a). These networks contribute to relaxing the γ/γ′ misfit effectively and retarding the cutting of dislocations into the γ′ precipitates[20, 21]. In contrast, during [111] tensile deformation, a maximum of six microscopic octahedral slip systems are indicated to be activated with a low Schmid factor (approximately 0.31). It results in the sluggish development of dislocation networks around γ′ particles, as shown in Figs. 3(c) and 4(c), which weakens the resistance of γ′ precipitates to the glide of matrix dislocations to some extent.

## 4.2 Influence of stress level on stress-rupture behavior

At the early stage of [001] tensile deformation, the plate-like γ/γ′ rafts form rapidly, and simultaneously, the (001) γ channels widen quickly due to the facilitation effect of slip-climb motion of dislocations with a 60° character along γ/γ′ interfaces on the rafting kinetics of γ′ precipitates[22]. The subsequent deformation in the lamella γ/γ′ structure is closely associated with two fundamental processes: (1) the enhanced mobility of matrix dislocation within the (001) γ channel, and (2) the slip-climb movements of dislocations along the interface of γ/γ′ rafts. Correspondingly, the dynamic recovery process is primarily governed by the diffusion of a supersaturated concentration of vacancies, which are generated as by-products of the slip-climb motion of mixed-character dislocations along semi-coherent γ/γ′ interfaces. These vacancies migrate toward growing micropores, facilitated by dislocation interactions. As deformation progresses further, an increasing density of dislocations with diverse Burgers vectors is driven into the γ′ precipitates, including those with single Burgers vectors of *a*/2<101>, *a*<101>, and *a*<010> (e.g., Refs. [23, 24]). The increase in applied stress increases the activity of matrix glide within the lamella structures and accelerates the occurrence of γ′-cutting events, which subsequently decreases the experimental endurance as expected. This is in line with the previous interpretations[25, 26]. The highly localized fracture behavior, resulting from a great number of γ′-cutting events, is closely related to the nucleation and growth of micropores due to the condensation of excessive vacancies in the lamella γ/γ′ structure, which depends primarily on temperature (e.g., Ref. [19]). This might be the reason why the facture plasticity is nearly identical under different stresses.

As for [111] applied loading, the multiplication of dislocations can be initially activated between the cuboidal γ′ precipitates when the Orowan barrier is overcome. It is indicated that the Orowan barrier is conversely proportional to γ channel width[16]. The mobility of matrix dislocations becomes easier as the γ channels gradually widen, as a result of the Ostwald ripening of γ′ precipitates. Subsequently, a growing number of dislocations are tangled with the coarsened γ′ precipitates. Finally, the high number of γ′-cutting events is attributed to the presence of a higher density of long dislocations deposited at γ/γ′ interfaces where the dislocation networks are poorly developed. In the dispersed γ/γ′ structure, the controlling dynamic recoveries include dislocation annihilation at the corners and dislocations cutting into γ′ precipitates. Both processes are sensitive to temperature and stress. Therefore, with the increasing stress level, the lifetime obtained after fracture is obviously decreased while the plasticity is largely increased. This is consistent with the finding that the fracture morphology is obviously sensitive to the applied load.

# 5 Conclusions

This study investigated the stress-rupture behavior and related heat-treated microstructure of a Ni-based single crystal superalloy in [001] and [111] directions under loadings of 100 MPa and 137 MPa at 1,100 °C. The following conclusions can be drawn:

(1) As the stress rises from 100 MPa to 137 MPa, the rupture lifetime is significantly reduced in [111]-orientated specimens and decreased in [001]-orientated specimens.

(2) The rupture lifetime is longer for [111]-oriented specimens than for [001]-oriented specimens under low-stress conditions; however, this trend is reversed under high-stress conditions.

(3) The initial microstructure transformes into a lamella γ/γ′ structure after the fast γ′ rafting in [001]-orientated specimens under stress conditions. In contrast, coarsened γ′ precipitates remain embedded in the γ matrix in [111]-orientated specimens.

(4) The fundamental deformation processes governing stress-rupture behavior in [001]-oriented specimens include the slip-climb motion of interfacial dislocations and the activity of matrix glide within the lamellar γ/γ′ raft structure.

(5) The deformation mechanisms in [111]-orientated specimens involve the mobility of dislocation loops through continuous γ channels once the Orowan resistance is overcome, followed by the γ′-cutting events by dislocations.

## Acknowledgments

This work was financially supported by the National Science and Technology Major Project of China (No. 2019-VII-0019-0161 and No. 2019-VII-0004-0144), the National Natural Science Foundation of China (No. 92360302), and the Shandong Provincial Natural Science Foundation of China (No. ZR2021QE103).

## Conflict of interest

The authors declare that they have no conflict of interest.

## References

[1] Reed R C. Superalloys: Foundations and applications. Cambridge: Cambridge University Press, 2006.

[2] Dye D, Ma A, Reed R C. Numerical modelling of creep deformation in a CMSX-4 single crystal superalloy turbine blade. Superalloys 2008, 2008: 911–919.

[3] Han G M, Yu J J, Sun Y L, et al. Anisotropic stress rupture properties of the nickel-base single crystal superalloy SRR99. Materials Science and Engineering: A, 2010, 527: 5383–5390.

[4] Li Y, Wang L, Zhang G, et al. Creep anisotropy of a 3rd generation nickel-base single crystal superalloy at 850 °C. Materials Science & Engineering: A, 2019, 760: 26–36.

[5] Liu J, Jin T, Sun X, et al. Anisotropy of stress rupture properties of a Ni base single crystal superalloy at two temperatures. Materials Science and Engineering: A, 2008, 479: 277–284.

[6] Caron P, Ohta Y, Nakagawa Y G, et al. Creep deformation anisotropy in single crystal superalloys. Superalloys 1988, 1988: 215–224.

[7] Sass V, Glatzel U, Feller-Kniepmeier M. Anisotropic creep properties of the nickel-base superalloy CMSX-4. Acta Materialia, 1996, 44: 1967–1977.

[8] Yu H, Su Y, Tian N, et al. Microstructure evolution and creep behavior of a [111] oriented single crystal nickel-based superalloy during tensile creep. Materials Science and Engineering: A, 2013, 565: 292–300.

[9] Wang G, Liu J, Liu J, et al. High temperature stress rupture anisotropy of a Ni-based single crystal superalloy. Journal of Materials Science & Technology, 2016, 32: 1003–1007.

[10] Agudo Jacome L, Nortershauser P, Heyer J K, et al. High-temperature and low-stress creep anisotropy of single-crystal superalloys. Acta Materialia, 2013, 61: 2926–2943.

[11] Agudo Jacome L, Nortershauser P, Somsen C, et al. On the nature of γ' phase cutting and its effect on high temperature and low stress creep anisotropy of Ni-based single crystal superalloys. Acta Materialia, 2014, 69: 246–264.

[12] Wang G, Liu J, Liu J, et al. Effect of orientation on stress-rupture property and related deformation microstructure of a Ni-base Re-containing single-crystal superalloy at 900 °C. Acta Metallurgica Sinica (English Letters), 2021, 34: 719–728.

[13] Bruckner U, Epishin A, Link T. Local X-ray diffraction analysis of the structure of dendrites in sin gle-crystal nickel-base superalloys. Acta Materialia, 1997, 45(12): 5223–5231.

[14] Sarosi P M, Srinivasan R, Eggeler G F, et al. Observations of a<010> dislocations during the high-temperature creep of Ni-based superalloy single crystals deformed along the [001] orientation. Acta Materialia, 2007, 55: 2509–2518.

[15] Link T, Epishin A, Klaus M, et al. <010> dislocations in nickel-base superalloys: Formation and role in creep deformation. Materials Science and Engineering: A, 2005, 405: 254–265.

[16] Muller L, Glatzel U, Feller-Kniepmeier M. Calculation of the internal stresses and strains in the microstructure of a single crystal nickel-base superalloy during creep. Acta Metallurgica et Materialia, 1993, 41: 3401–3411.

[17] Volkl R, Glatzel U, Feller-Kniepmeier M. Analysis of matrix and interfacial dislocations in the nickel-base superalloy CMSX-4 after creep in [111] direction. Scripta Metallurgica et Materialia, 1994, 31: 1481–1486.

[18] Pollock T M, Argon A S. Creep resistance of CMSX-3 nickel-base superalloy single-crystals. Acta Metallurgica et Materialia, 1992, 40: 1–30.

[19] Epishin A, Link T. Mechanisms of high-temperature creep of nickel-based superalloys under low applied stresses. Philosophical Magazine, 2004, 84: 1979–2000.

[20] Tanaka K, Ichitsubo T, Kishida K, et al. Elastic instability condition of the raft structure during creep deformation in nickel-base superalloys. Acta Materialia, 2008, 56: 3786–3790.

[21] Inoue T, Tanaka K, Adachi H, et al. Evolution of orientation distributions of gamma and γ' phases during creep deformation of Ni-base single crystal superalloys. Acta Materialia, 2009, 57: 1078–1085.

[22] Qi D, Wang L, Zhao P, et al. Facilitating effect of interfacial grooves on the rafting of nickel-based single crystal superalloy at high temperature. Scripta Materialia, 2019, 167: 71–75.

[23] Tang Y, Huang M, Xiong J, et al. Evolution of superdislocation structures during tertiary creep of a nickel-based single-crystal superalloy at high temperature and low stress. Acta Materialia, 2017, 126: 336–345.

[24] Zhang J X, Murakumo T, Koizumi Y, et al. Slip geometry of dislocations related to cutting of the γ' phase in a new generation single-crystal superalloy. Acta Materialia, 2003, 51: 5073–5081.

[25] Mughrabi H, Biermann H, Ungar T. X-ray analysis of creep induced local lattice parameter changes in a monocrystalline nickel-base superalloy. Superalloys 1992, 1992: 599–608.

[26] Link T, Epishin A, Bruckner U, et al. Increase of misfit during creep of superalloys and its correlation with deformation. Acta Materialia, 2000, 48: 1981–1994.